# An insight into the heat-management for the $CO_2$ methanation based on free convection

A. Alarcón[a,b], J. Guilera[a*] and T. Andreu[a]

[a]Catalonia Institute for Energy Research (IREC), Jardins de les Dones de Negre 1, 08930 Sant Adrià de Besòs, Spain

[b]Escuela Superior Politécnica del Litoral, ESPOL, Facultad de Ingeniería en Ciencias de la Tierra, Campus Gustavo Galindo Km.30.5 Vía Perimetral, P.O. Box 09-01-5863, Guayaquil, Ecuador.

*corresponding author: jguilera@irec.cat

## Abstract

This article presents a novel heat-management approach for $CO_2$ valorization to synthetic natural gas based on free convection to the environment, without requirements of heat-exchange services. With this aim, a reactor channel was built (d=4.6 mm, L=250 mm) and tested at different conditions of inlet temperatures, gas hourly space velocities and pressures using an active nickel/ceria-based catalyst. After experimentation, a CFD model was developed, validated and employed for an efficient sensitive analysis of the most suitable reaction conditions. The simulation criteria were high $CO_2$ conversion level and restrict overheating to avoid catalyst and reactor degradation. Then, the optimal conditions found by CFD modelling were successfully validated at lab-scale. The $CO_2$ conversion level experimentally obtained was 93%, by using a decreasing temperature profile in the range of 830-495 K, operating at a pressure of 5 atm and a gas hourly space velocity of 11,520 $h^{-1}$. The proposed reactor configuration guarantees an efficient heat management along the reactor channel by using feasible conditions of pressure, temperature and flowrate for its implementation in small-scale applications, where the use of the exothermic heat is less profitable.

**Keywords:** $CO_2$ methanation; synthetic natural gas; reactor design, heat-management; computational fluid dynamics

## 1. Introduction

The synthesis of synthetic methane through carbon dioxide ($CO_2$) methanation reaction has high interest in the context of Power-to-Gas (PtG) [1–6]. The methanation reaction allows to store the intermittent electricity production derived from renewable energy sources [7,8]; and besides it allows the valorization of carbon dioxide to renewable natural gas [9–12]. The starting point of the overall PtG process is the utilization of renewable electricity to produce green hydrogen ($H_2$) through water electrolysis. Then, in an additional processing step, the formed $H_2$ is combined with $CO_2$ and converted to methane ($CH_4$). In this way, the energy carrier is in the form of $CH_4$, which is the main compound of natural gas. Hence, this product is known as synthetic natural gas (SNG). The main advantage of SNG, in comparison with other synthetic fuels, is that it can be fed into the existing gas infrastructure without any limitations or any further processing. This is a clear advantage as transportation using pipelines is more energy-efficient and environmentally friendly than road transport.

The thermochemical $CO_2$ methanation process is carried out through Sabatier reaction (Eq.1). This reaction is reversible, exothermic and thermodynamically favoured at low temperatures and high pressures. As kinetics of the reaction are limited at the mentioned conditions, an active catalytic system is required to obtain SNG at reasonable reaction times. Most works on catalyst design for this reaction are based on noble- and transition-metal materials (Ru, Rh, Pd and Ni) supported on metal oxides ($Al_2O_3$, $CeO_2$, $ZrO_2$, $TiO_2$, $SiO_2$, $La_2O_3$ or combination between them) [13,14]. In recent times, it has been reported that the modification of the support through the incorporation of promoters ($CeO_2$, $La_2O_3$, $Pr_2O_3$, $Gd_2O_3$, $ZrO_2$, $MnO_2$ and MgO) improves the catalyst stability and even tolerance to industrial impurities [15–19].

$$CO_{2(g)} + 4H_{2(g)} \rightleftharpoons CH_{4(g)} + 2H_2O_{(g)} \qquad \Delta H^{o}_{298K} = -165\ \mathrm{kJ \cdot mol^{-1}} \qquad \text{Eq.1}$$

Beyond catalyst advances, the design of a reactor with efficient heat removal is another challenge to face in $CO_2$ methanation technology, especially for decentralized application. Catalytic reactors, such multi-tubular fixed-bed [20–26], microchannel [27], fluidized bed [28], stirred-tank slurry [29], microstructured [30–37], honeycomb [38] and compact wall [39] are interesting approaches able to conduct the Sabatier reaction. Among them, the fixed-bed reactor tube coupled with an oil cooling system was already implemented at industrial level already in 2013 [40]. Recent advances are related to the utilization of micro- or milli- size reactor for process intensification and temperature control. Miniaturized packed-bed reactors exhibit unique heat and mass transfer characteristics because of high surface-to-volume ratios [41]. Higher heat transfer capacity is achieved by decreasing the inner channel dimensions. Consequently, it was inferred that micro-reactors work at much higher gas flowrates than conventional units [42]. However, the heat generated from the Sabatier reaction is typically released to another fluid by means of the incorporation of complex heat-management systems and several auxiliary devices.

A reactor configuration with a heat-management approach based on free convection is a promising alternative because then the reactor engineering is significantly simplified [43]. As Sabatier reaction is an exothermic process, the released heat can be controlled by some reaction parameters and heat can be released to the environment without the implementation of intensive cooling systems [44]. A free convection heat transfer to the surroundings for the reactor cooling can be a technological alternative for lowering the investment costs in small-size plants. Note that the definition of this novel reactor approach differs from an autothermal approach, as in this second case, the cooling is performed in-situ by an endothermic reaction; e.g. autothermal steam reformers [45]. This “simple as possible” strategy is interesting approach to expand the application of $CO_2$ methanation in decentralized locations with low production capacity, where it has been demonstrated that high investments are not profitable.

The operation of reactor using polytropic temperature profiles is required to achieve high SNG productions in smaller volumes [21,23] . Recently, Moioli et al.[46] proposed a model-based determination of the optimal reactor concept for Sabatier reaction by controlling the heat transfer. They found that the reactor can be divided into three zones: an initial zone for reaction activation, a central zone to remove excess heat and a final zone to reach the thermodynamic equilibrium curve. For an unsteady state and

more flexible process operation, also known as dynamic operation, Bremer et al.[47] applied stabilizing control to moderate the reactive zone (hot spot) via adaptive coolant temperature variations. They suggested that through this strategy is possible to obtain unconventional operating points in regions of steady-state multiplicity that offer reduced catalyst temperature, while maintaining elevated reactor performance. In another study, Zhang et al.[48] developed a steady-state solver based on the open-source toolbox. The numerical study proposed heat transfer between the reacting gas in a porous catalyst layer, reactor tube, and coolant in a shell-and-tube reactor. They concluded that through the computational fluid dynamic simulations was possible to predict the trends of temperature profiles both in axial and radial directions. Therefore, computational fluid dynamic (CFD) modelling seems a powerful tool for reactor design and specially to avoid experimental trial-and-error methodologies.

The aim of this work is to propose a simple heat-management reactor configuration based on free convection to the environment for lowering the overall investment costs in decentralized small-scale $CO_2$ methanation units. With this aim, a combination of experimentation on a reactor channel (diameter of 4.6 mm and length of 250 mm) and CFD simulation was carried out. The reaction conditions ($T_{inlet}$, GHSV, P), in which the proposed configuration is able to operate without the use of external cooling/heating systems and to achieve a high $CO_2$ conversion level (≥90%) are hereby presented. The scale-up of the reactor approach considering a representative industrial small-scale $CO_2$ methanation case (1 $Nm^3 \cdot h^{-1}$ of SNG production) together with the main advantages and disadvantages of this heat-management configuration are further discussed.

## 2. Experimental

### 2.1. Catalyst preparation

The catalyst used in this study was a ternary catalytic system based on Ni as active phase (25 wt.%), $CeO_2$ as promoter (20 wt.%) and $\gamma$-$Al_2O_3$ micro-spheres as support (55 wt.%). Catalyst design, synthesis and formulation was optimized in previous works [49,50] and validated in a relevant environment [42]. Specifications of the catalyst can be found in those publications. To summarize, 50 g batch was prepared by dissolving salt precursors of nickel (II) nitrate hexahydrate ([$Ni(NO_3)_2 \cdot 6H_2O$] with 98% purity, Alfa Aesaer) and cerium (III) nitrate hexahydrate ([$Ce(NO_3)_3 \cdot 6H_2O$] with 99% purity, Fluka) in distilled water. Then, the aqueous solution was mixed with $\gamma$-$Al_2O_3$ commercial support in shape of microspheres with particle diameters $d_p$=450-500 μm (NorPro Saint-Gobain), on a rotary vacuum evaporator with constant stirring (25 rpm) at room temperature for 1 h. Subsequently, the solvent was in-situ evaporated at 358 K and P=0.8 bar·g for 6 h. Finally, the impregnated micro-spheres were first dried overnight at 378 K and then calcined at 723 K for 30 min with a heating ramp of 1 $K \cdot min^{-1}$.

### 2.2. Experimental setup

$CO_2$ methanation reaction was conducted in the homemade reactor setup, illustrated in Figure 1. The gases $H_2/CO_2$ mixture (99.999%, Linde) and $H_2$ (99.999%, Linde) were supplied through a set of mass flow controllers (MFC, Bronkhorst). A heating tape (Omegalux) monitored by a thermoregulation system (Horst GmbH) was used to pre-heat the gas mixture to the desired temperature. Reactor channel dimensions

(inner diameter of 4.6 mm and length of 250 mm) were selected to facilitate the heat transfer to the environment, as it is highly promoted when the inner diameter is reduced from 10 mm [51]. The tube was filled with approximately 3.52 g of catalyst. Temperature was measured by six type K thermocouples (1/16 in, Omega Engineering Inc.); two of them were placed outside of the reactive zone (inlet and outlet of the reactor) and four along the reactive zone (axial position of 28, 53, 99 and 188 mm). Fiberglass tape, 40 mm mineral wool and aluminum foil was used to insulate the reactor. Pressure was regulated by a manual valve placed at the outlet. Then, the unconverted gases and the reaction products leaving the reactor were cooled down to 278 K by using a circulation chiller (VWR,1160S model) and cold liquid-gas separator to condense and trap water produced, respectively. Prior to the analysis of the composition of the gases, a coalescence filter (Classic filter, SS127.221-C-5CS model) was additionally used to ensure the total water removal. At this point, the dry gas flow was measured by a flow meter (FM, Bronkhorst) and its composition was successively analysed by an on-line gas micro-chromatograph (490 microGC, Agilent Technologies). This was equipped with three columns, two molecular sieve (MS5A) for $H_2$, Ar, $N_2$, CO and $CH_4$ analysis, one porous polymer (PPU) for $CO_2$ and light hydrocarbons. Each column is followed by a thermal conductivity detector (TCD).

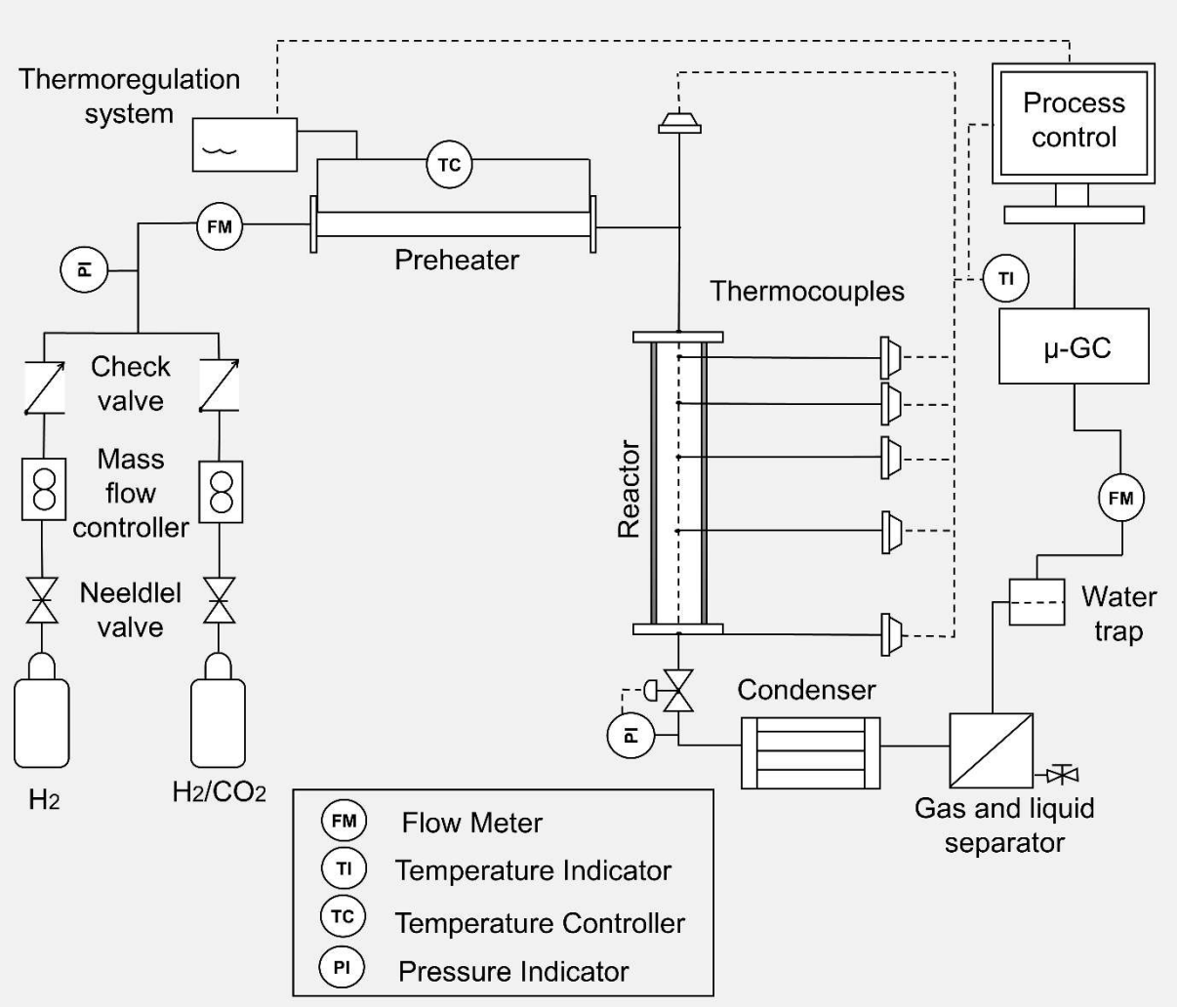


Figure 1. Schematic illustration of the reactor testing setup.

### 2.3. Procedure

Prior to reactor start-up, catalyst was reduced in a tubular furnace using 5 vol% $H_2$/Ar at a flowrate of 100 mL·min$^{-1}$. The temperature was increased up to 773 K for 3 h with a heating ramp of 1 K·min$^{-1}$, followed by a cooled-down to room temperature. Then, the catalytic bed was filled with the reduced catalyst. Experiments were conducted in the range of P=1-5 atm, $T_{inlet}$=503-573 K, a stoichiometric $H_2/CO_2$ ratio of 4 and using gas hourly spacy velocities (GHSVs) in the range from 3,039 to 18,235 h$^{-1}$. GHSV was calculated by Eq. 2:

$$GHSV = \frac{F}{\frac{m_{Cat.}}{\rho_{Cat.}}} \quad \text{Eq. 2}$$

where $F$ is inlet gas mixture, in the range from 200 to 1,200 NmL·min$^{-1}$, $m_{Cat.}$ is the catalyst mass (3.52 g) and $\rho_{Cat.}$=0.891 $g_{cat.}$·mL$^{-1}$ is the measured catalyst density. The performance of the process was evaluated through $CO_2$ conversion (Eq. 3), $CH_4$ selectivity (Eq. 4) and $CH_4$ productivity rate (Eq. 5).

$$X_{CO2}\,[\%] = \frac{n_{CO2,in} - n_{CO2,out}}{n_{CO2,out}} * 100 \quad \text{Eq. 3}$$

$$S_{CH_4} = \frac{n_{CH4,out}}{n_{CH4,out} + n_{CO,out}} * 100 \quad \text{Eq. 4}$$

$$rCH_4[mol \cdot h^{-1} \cdot kg^{-1}] = \frac{n_{CH4,out}}{m_{Cat}} \quad \text{Eq. 5}$$

where $n_j$ represents the molar flow rate of species j (j=$CO_2$ and $CH_4$) in the inlet and outlet gas. Sub-products, such as CO and $C_{2+}$ hydrocarbons were not detected. Therefore, methane selectivity was close to 100%. As a representative example, Figure SI1-3 show raw chromatograms of the analytics, confirming complete selectivity to $CH_4$ formation.

## 3. CFD model

The CFD model proposed in this work was developed using the Ansys®Fluent software, 2019 R2 version. The geometry used for simulation presented the same dimensions than the lab-scale reactor. A schematic representation of the methanation reactor is shown in Figure 2. In the modelling, the length of the reactor was divided into five symmetric sections of 50 mm ($LS_{i=1-5}$) to adjust individual heat transfer rates along the reactor tube.

A dynamic meshing design of the 3D geometry model was created with a total of six cell zones using 43,078 nodes. One cell zone was identified as the reactive zone with homogeneous porous medium composed by catalyst and gas mixture and the others five as solid zones. Eight principal zones were also defined as boundary conditions: the gas inlet mixture, the gas outlet mixture, the tube length sections ($LS_{i=1-5}$), and the interface. The set of partial differential equations involved in the mathematical model were derived from the integration of three sub-models: i) energy, ii) species transport, and iii) viscous. The governing equations of the Ansys®Fluent software can be found in the Appendix of the Supporting Information.

The apparent kinetic parameters were obtained in a previous work [51]. Two empirical power law rate expressions were used of the forward and the backward reaction, presuming arbitrary orders only for $CO_2$ and $H_2$ (Eq. 7 and 8), while reverse water gas shift reaction was neglected in the model. A more detailed experimental kinetic study on this catalyst could improve adjust of the kinetic model to experimental conditions. For instance, by assessing the influence of $CH_4$ and $H_2O$ products to the kinetics and to evaluate the influence of CO formation in the model.

Kinetic expression for forward reaction

$$r_f(\mathrm{mol}\cdot\mathrm{m}^{-3}\cdot\mathrm{s}^{-1}) = 8.38\cdot10^{7}\mathrm{e}^{-6.20\cdot10^{7}/\mathrm{RT}}\cdot(\mathrm{C_{CO2}})^{0.171}\cdot(\mathrm{C_{H2}})^{0.683} \quad \text{Eq. 6}$$

Kinetic expression for backward reaction

$$r_b(\mathrm{mol}\cdot\mathrm{m}^{-3}\cdot\mathrm{s}^{-1}) = 8.78\cdot10^{17}\mathrm{e}^{-2.33\cdot10^{8}/\mathrm{RT}}\cdot(\mathrm{C_{CO2}})^{-0.829}\cdot(\mathrm{C_{H2}})^{-3.316} \quad \text{Eq. 7}$$

The physical properties for the reactive zone (rz), such as specific heat ($C_{prz}$=6,433 $J\cdot kg^{-1}\cdot K^{-1}$), thermal conductivity ($\lambda_{rz}$=0.34 $W\cdot m^{-1}\cdot K^{-1}$) and viscosity ($\mu_{rz}$=1.23·$10^{-06}$ $kg\cdot m^{-1}\cdot K^{-1}$) were obtained through the NIST data base [52] and defined as constant values. The species ($H_2$, $CO_2$, $CH_4$ and $H_2O$) were modelled as ideal gas and their mass diffusivity were calculated by the kinetic theory. Steel was selected as material of the reactor tube and its thermal conductivity ($\lambda_S$) was 16.27 $W\cdot m^{-1}\cdot K^{-1}$. Newton's law of cooling (Eq. 8) was used to model the convective heat loss to the surroundings from the outer wall.

$$\dot{q} = h\Delta T = h(T_{outerwall} - T_{\infty}) \quad \text{Eq. 8}$$

where $\dot{q}$ is the heat flux density [$W\cdot m^{-2}$], $h$ is the free convective heat coefficient of the fluid [$W\cdot m^{-2}\cdot K^{-1}$] and $\Delta T$ is the temperature difference [K] between outer wall temperature ($T_{outerwall}$) and the bulk temperature ($T_{\infty}$). The heat flux, $\dot{q}$, for each reactor section was estimated assuming a bulk temperature of 298 K and considering the temperature connexion between reactive zone, tube innerwall as well as tube outerwall. Temperature behaviour between them was simulated by using a coupling tool under the assumption that the reduction of temperature was from reactive zone to tube outerwall.

The reactor modelling was carried out under the following assumption: the gas mixture was preheated to the inlet temperature, the gas velocity was uniform, the operating pressure was defined at outlet reactor tube, the pressure drop along the axial reactor coordinate was neglected and the heat of the reaction was transferred at the pipe wall to the surroundings. A summary of reactor dimensions, properties and operating parameters used in the simulations are presented in Table 1. The set of partial equations were solved by the pressure-based Navier-Stokes algorithm with a steady-state time dependence. The pressure-velocity coupling with a Simplec scheme was selected as solution methods. The number of iterations used in each simulation was 2000.

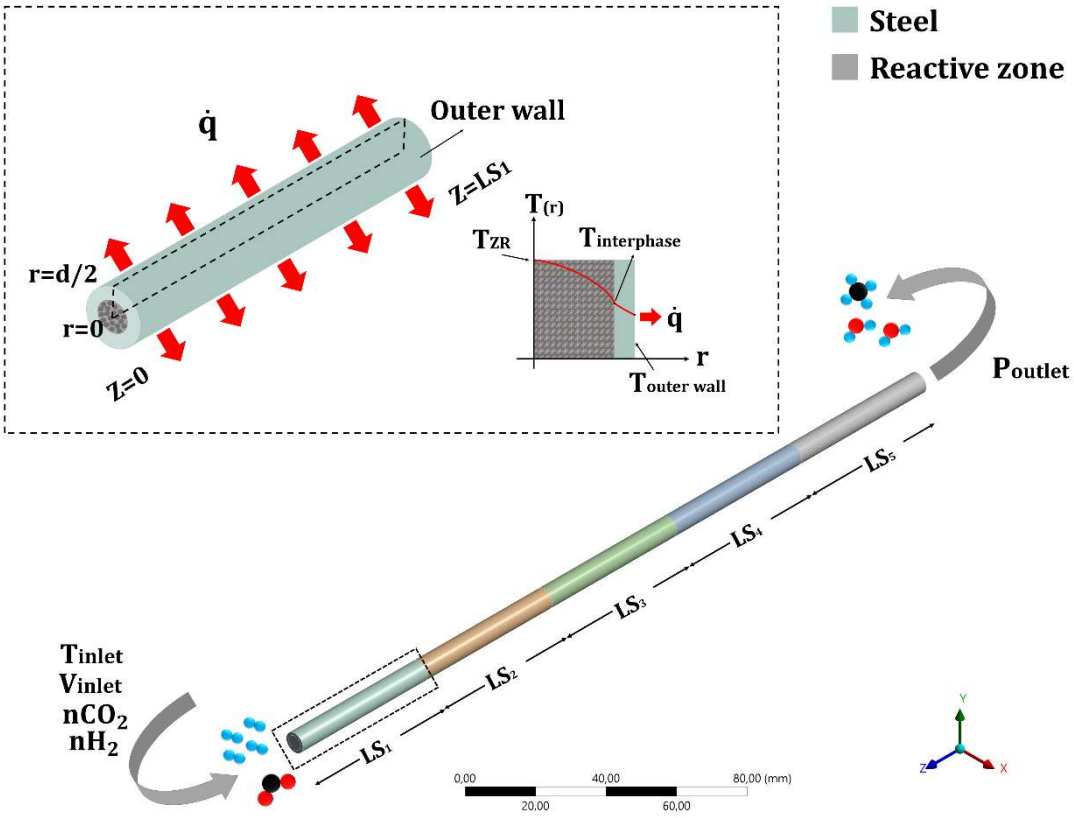


Figure 2. Geometry design of the fixed-bed reactor tube used on CFD model.

Table 1. Summary of reactor dimensions, properties and operating parameters used on the CFD model.

| Reactor dimension | Symbol | Value | Unit |
|---|---|---|---|
| Inner diameter | $D_i$ | 4.6 | mm |
| Outer diameter | $D_o$ | 6.4 | mm |
| Length | L | 250 | mm |
| Length sections | $LS_{i=1-5}$ | 50 | mm |
| **Property** | **Symbol** | **Value** | **Unit** |
| Thermal conductivity of the steel reactor tube | $\lambda_s$ | 16.27 | $W \cdot m^{-1} \cdot K^{-1}$ |
| Specific heat of the reactive zone[a] | $C_{prz}$ | 6,433 | $J \cdot kg^{-1} \cdot K^{-1}$ |
| Thermal conductivity of the reactive zone[a] | $\lambda_{rz}$ | 0.34 | $W \cdot m^{-1} \cdot K^{-1}$ |
| Viscosity of the reactive zone[a] | $\mu_{rz}$ | $1.23 \cdot 10^{-06}$ | $kg \cdot m^{-1} \cdot K^{-1}$ |
| Temperature of the exterior | $T_{?}$ | 298 | K |
| Heat transfer coefficient of air[b] | $h_{air}$ | 19.45 | $W \cdot m^{-2} \cdot K^{-1}$ |
| **Operating parameter** | **Symbol** | **Value** | **Unit** |
| Molar ratio of $H_2/CO_2$ | - | 4 | - |
| Mole fraction of $H_2$ | $\dot{m}_{H2}$ | 80 | % |

| | | | |
|---|---|---|---|
| Mole fraction of $CO_2$ | $\dot{m}co_2$ | 20 | % |
| Temperature of the inlet | $T_{inlet}$ | 473-673 | K |
| Pressure | P | 1-20 | atm |
| Gas hourly space velocity | GHSV | 6,834 -13,676 | $h^{-1}$ |

[a] Calculated using NIST data base.
[b] Calculated at $V_{air}$=1m·$s^{-1}$ to guarantee a free convection.

## 4. Result and discussion

### 4.1. $CO_2$ methanation tests

The first $CO_2$ methanation tests were conducted in the reactor setup by varying the gas flowrate in the range of GHSV=3,039-18,235 $h^{-1}$ at atmospheric pressure. The reaction start-up was carried out by pre-heating of inlet gas at $T_{inlet}$ of 573 K. As soon as the reaction started, temperatures along the reactor increased gradually due to the exothermicity of the methanation reaction. Steady-state conditions were obtained after 35-85 min, depending on the used gas flowrate. The maximum temperature of the reactor was self-restricted at $T_{max}$≤823 K to avoid catalyst degradation by limiting the inlet gas flowrates.

As it can be observed in Figure 3, non-isothermal temperature profiles were always obtained. The operation using decreasing temperature profiles is preferred to isothermal operation to reduce the reactor volume by a compromise of kinetics and equilibrium conditions [53]. Otherwise, in isothermal operation, a higher temperature can lead to equilibrium restrictions and lower temperature to kinetics ones. The highest temperatures ($T_{max}$=673-806 K) were detected close to the reactor inlet (axial position 28 mm) and the lowest ones ($T_{min}$=310-378 K) were recorded at the reactor outlet (axial position 250 mm). This first series of experiments revealed that higher temperatures along the reactor were obtained at higher GHSV values. Accordingly, it was confirmed that a simple way to control the temperature profile in the proposed reactor heat-management configuration is by adjusting the inlet gas flowrate. In such a way that the reactor can be heated up by increasing the gas flowrate and cooled-down by lowering it.

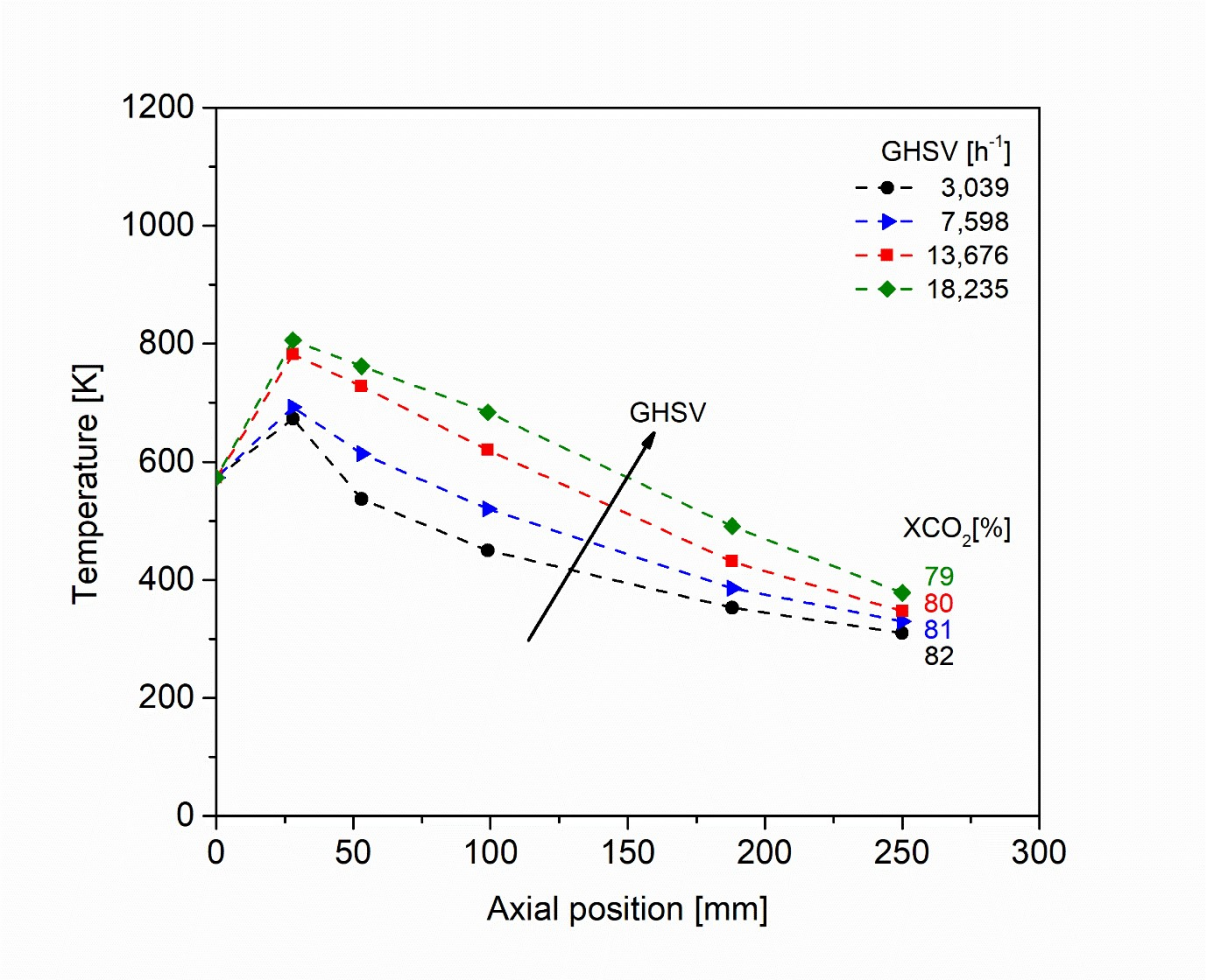


Figure 3. Experimental temperature profiles by varying GHSV at P=1 atm and $T_{inlet}$=573 K.

At the tested conditions, $CO_2$ conversions slightly decreased from 82 to 79% by increasing the GHSV from 3,039 to 18,235 $h^{-1}$. In this aspect, the decrease of the conversion (-3%) was really low compared to the reduction of the gas residence time in the reactor (-88%). The $CO_2$ conversion pattern was a consequence of two opposite effects; high GHSV led to higher reaction temperatures but lower residence times for reaction. As observed, the operation at higher temperatures was more decisive than lowering the gas residence time. This behaviour is probably a consequence that kinetic values depend exponentially on the temperature, while residence time does not have this strong dependence on the reaction rates. In any case, the maximum experimental $CO_2$ conversion achieved during this first set of experiments was 82%.

The achieved level of conversion is still too low for industrial applications [53], and out of the scope of the present work (≥90%). An experimental alternative to achieve conversion close (91-84%) to the equilibrium at these conditions was adjusting the temperatures by addition of external heat to the last zone of the reactor. In this second set of experiments (see Figure SI5), the most favorable conditions were obtained when the lowest temperature was higher than 573 K. Therefore, optimal conditions cannot be obtained by simply adjusting the inlet flowrate. A suitable and effective technique to obtain the optimum reaction conditions able to achieve a high conversion level is by CFD modelling.

### 4.2. CFD model validation

At first, the CFD model was validated using the experimental case carried out at P=1 atm, $T_{inlet}$=573 K and GHSV=13,676 $h^{-1}$. The parameters used in this simulation are described in Table 1. The length of the reactor was divided into five symmetric sections of 50 mm ($LS_{i=1-5}$) and the heat transfer values from the system to the surrounding were adjusted in each reaction zone. At the selected experimental condition, the amount of heat released to the surroundings was in the range of -[9,415–2,053] $W \cdot m^{-2}$. The amount of heat transferred was higher at the initial reaction zone and decreased along the reactor tube. This is a consequence of higher driving force, i.e. higher temperature difference between the system and the surroundings.

Figure 4 compares the experimental and the CFD simulation results. As can be seen, the temperature profile and the conversion level obtained from simulation were very close to the experimental results. The highest temperature ($T_{max}$=775 K) was detected close to the reactor inlet and the lowest temperature ($T_{min}$=358 K) at reactor outlet. Only small divergences were obtained in the conversion level (±2%). In fact, the lower experimental conversion ($X_{CO2}$=80%) can be a consequence of the lower temperature at the reactor outlet. Therefore, these results confirmed the suitability of the proposed CFD model to optimize the reactor parameters, as well as, to determine the heat fluxes of the proposed reactor design.

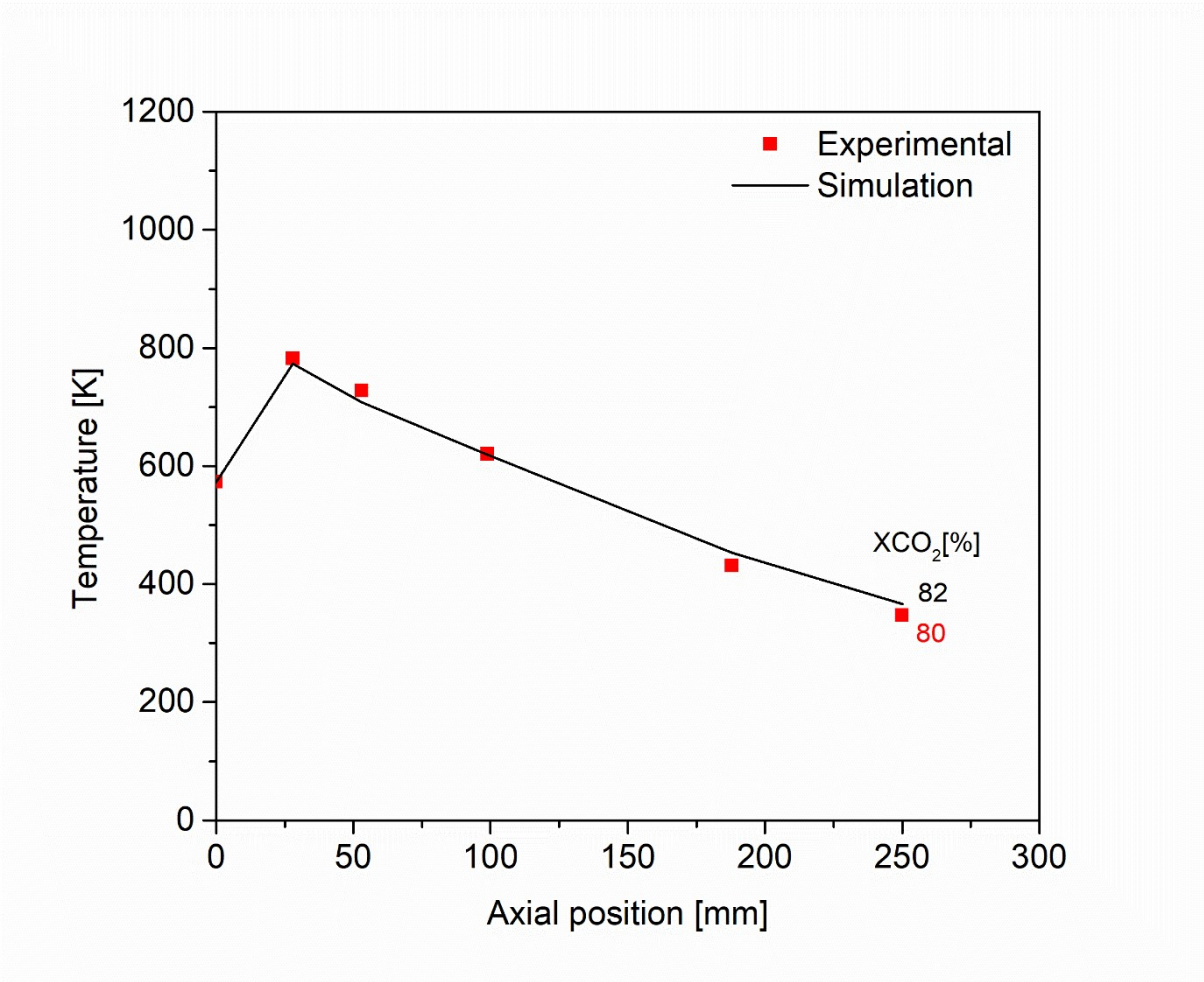

Figure 4. CFD model validation: comparison between experimental and simulated temperature profiles. Reaction conditions: GHSV=13,676 $h^{-1}$, $T_{inlet}$=573 K and P=1 atm.

### 4.3. Sensitive analysis of the reaction conditions

As the experimental results were successfully described by the developed CFD model, the influence of the operational parameters was further evaluated using this tool. The influence of P, $T_{inlet}$ and GHSV on temperature profile was studied in the range of 473-673 K, 1-20 atm and 6,837-13,676 $h^{-1}$, respectively. The sensitive analysis of the reaction parameters was performed using the following 2 criteria i) $CO_2$ conversion higher than 90%, ii) maximum temperature lower than 830 K. A total of 29 reactor configuration were studied. All simulation results are summarized in the Table S1.

As representative example, the influence of the pressure on temperature profiles at $T_{inlet}$=573 K and GHSV=13,676 $h^{-1}$ is displayed in Figure 5. Note that solid lines are used in the graphs for the conditions that met these criteria, while dashed for those that do not. As a general rule, it was observed that temperatures along the reactor was increased when the pressure was higher. Furthermore, the increase of pressure impacted highly positive to the conversion, attaining 91% at 5 atm. In contrast, a significant reduction on the $CO_2$ conversion values (≤87%) was unexpectedly observed at high pressures (P≥10 atm). This pattern was related to the reaction equilibrium limits the conversion level at high temperatures ($T_{max}$>823 K), which are not favourable to produce $CH_4$ [54]. Therefore, this highlight allowed the identification of the optimal pressure condition in which the proposed catalytic system can achieve an efficient $CO_2$ conversion.

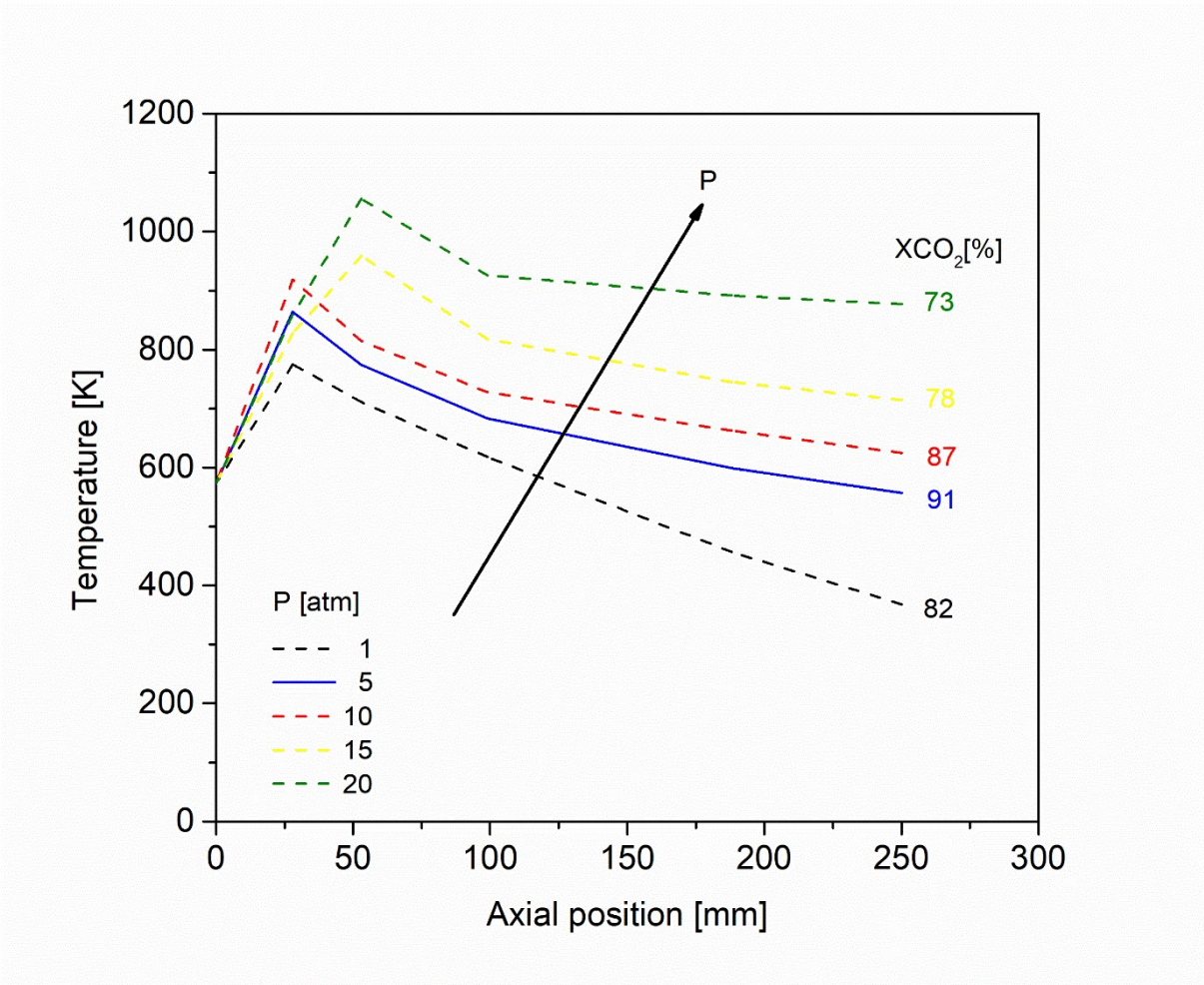


Figure 5. Influence of P on the temperature profile and the conversion level at GHSV=13,676 $h^{-1}$ and $T_{inlet}$=573 K obtained by CFD simulation.

The effect of the inlet temperature was evaluated at 5 atm and GHSV=13,676 $h^{-1}$ in order to avoid catalyst and reactor degradation due to overheating. The influence of the inlet temperature at those conditions is displayed in Figure 6, which suggests that the inlet temperature is a strategic parameter to control the formation of the hot spots ($T_{max}$) inside of the reactor. A reduction of the inlet temperature below 573 K was positive as increased the conversion level and decreased the overheating, even more molecules of methane were formed and thus more heat was released. At these conditions, the $T_{max}$ was lower than 823 K and $CO_2$ conversions were higher than 92%. These positive results can be related to thermodynamic reaction equilibrium. It well known that high pressures and low temperatures leads to high methane production.

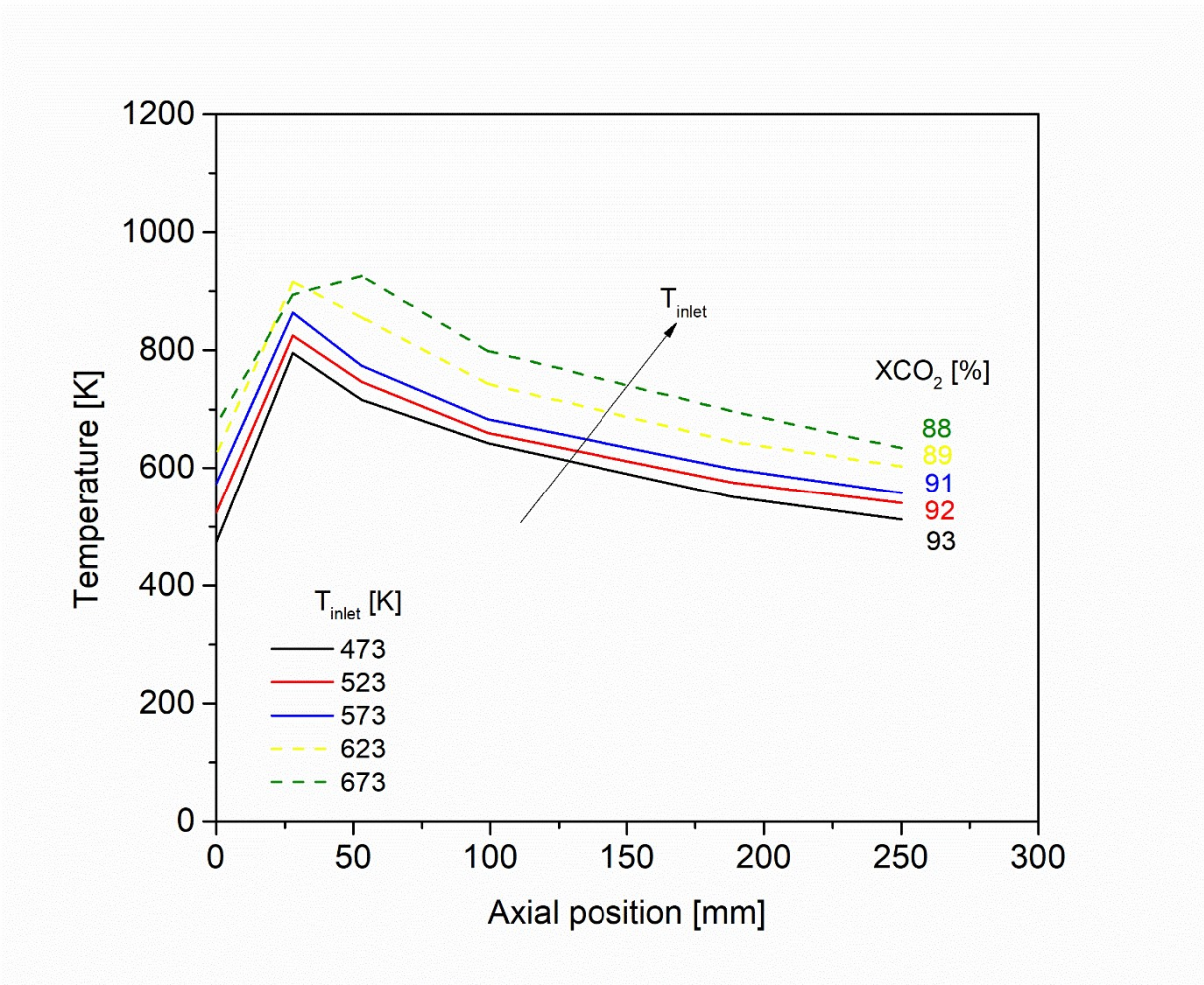


Figure 6. Influence of $T_{inlet}$ on the temperature profile and the conversion level at GHSV=13,676 $h^{-1}$ and P=5 atm obtained by CFD simulation.

The last parameter evaluated in the sensitive analysis was the GHSV. Figure 7 shows the temperatures along the reactor tube as a function of the GHSV values at $Ti_{nlet}$=523 K and P=5 atm. As it can be seen, the influence of the inlet GHSV was relevant in both the conversion and the temperature profiles. The highest level of conversion was achieved (97%) at the lowest GHSV (6,838 $h^{-1}$), despite the low reaction temperatures. From these results, it is inferred that the reactor can work, in principle, at GHSV values in the range of 12,307 $h^{-1}$≥GHSV≥8,205 $h^{-1}$ at 5 atm without the installation of neither a cooling nor a heating system. At these conditions, temperature of the reaction along the reactor tube can be controlled by the inlet flowrate. On one hand, operation at higher values (GHSV≥13,676 $h^{-1}$) demands of an external cooling system to restrict $T_{max}$≤823 K to avoid catalyst degradation. On the other hand, operation at low values (GHSV≤6,838 $h^{-1}$) demands of an external heating system at the last zone of the reactor to achieve high conversion values. The obtained heat fluxes from the simulations are presented in Table S2.

As mentioned, the target of the present reactor approach is to avoid external cooling and heating of the reactor channel. In short, CFD simulations showed that the conditions for $CO_2$ methanation can be reached by adjusting the gas flowrate and the

pressure. The operation at the potential zone (6,838 ≥GHSV≥13,676 $h^{-1}$) can be finally adjusted by the inlet temperature of the gases. As the reactor temperature rose with increasing the inlet temperature (see Figure 6), a slight decrease of the inlet temperature allows to work at higher GHSV values without exceeding the self-imposed limit temperature.

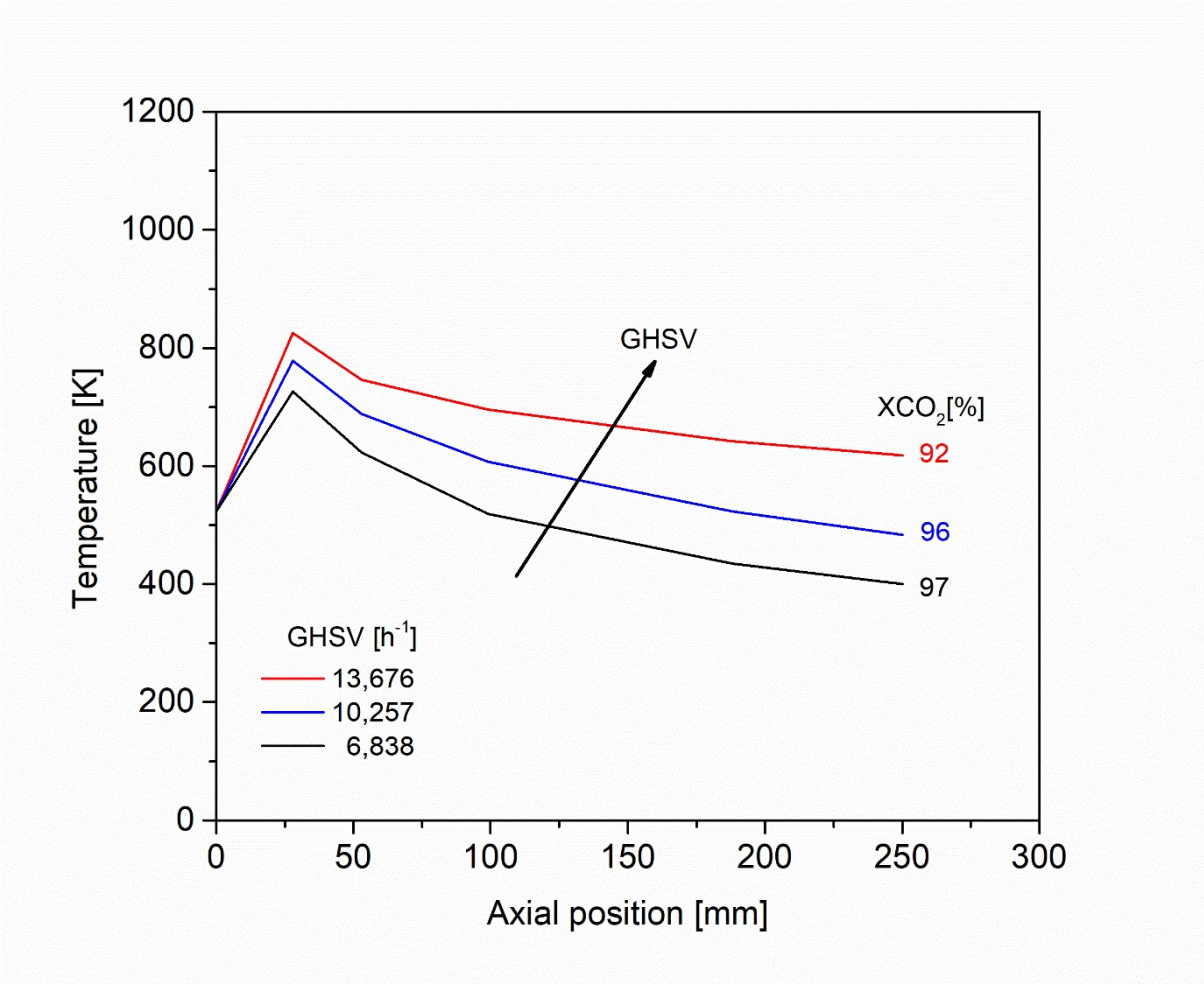


Figure 7. Influence of GHSV on the temperature profile and the conversion level at $T_{inlet}$=523 K and P=5atm obtained by CFD simulation.

### 4.4. Reaction conditions proposal

CFD simulations revealed that a compromise between kinetic, thermodynamic limitations and suitable heat-management is required to achieve high $CO_2$ conversions. In this aspect, the inlet temperature of the proposed reactor was set at 503 K and the pressure at 5 atm, the minimum values in which ≥90% of conversion was achieved. Both conditions are technically feasible in a relevant environment. On the other hand, a GHSV=11,520 $h^{-1}$ was selected considering the maximum GHSV, in which is possible the operation of the reactor without the implementation of an external cooling and heating system. The increase of the GHSV parameter benefits from a reduction of the necessary reactor volume. A summary of the operational conditions of the reactor design proposal are presented in Table 2.

Table 2. Design proposal for reactor.

| Operating parameter | Symbol | Value | Unit |
|---|---|---|---|
| Molar ratio of $H_2/CO_2$ | $H_2/CO_2$ | 4 | - |
| Mole fraction of $H_2$ | $\dot{m}_{H2}$ | 80 | % |
| Mole fraction of $CO_2$ | $\dot{m}co_2$ | 20 | % |
| Temperature of gas mixture | $T_{inlet}$ | 503 | K |
| Pressure | P | 5 | atm |
| Gas hourly space velocity | GHSV | 11,520 | $h^{-1}$ |
| Heat flux | $\dot{q}_{LS1}$ | 17,135 | $-W \cdot m^{-2}$ |
| | $\dot{q}_{LS2}$ | 15,229 | |
| | $\dot{q}_{LS3}$ | 12,979 | |
| | $\dot{q}_{LS4}$ | 11,055 | |
| | $\dot{q}_{LS5}$ | 9,900 | |

The temperature profile of the proposed configuration is displayed in Figure 8, which indicates the feasibility of this reactor approach. At the selected conditions, the simulated $CO_2$ conversion was 96% and the decreasing temperatures along the reactor tube was in the range of 817-505 K. The main effect of each parameter is described as follows. The temperature of gas pre-heating enables the restriction of the maximum temperature at the initial reaction zone and thus to avoid excessive hot-spots, GHSV allows the management of the reaction temperature along the reactor tube and to avoid external heating or cooling units, and finally, a compromise between the pressure leads to higher conversions.

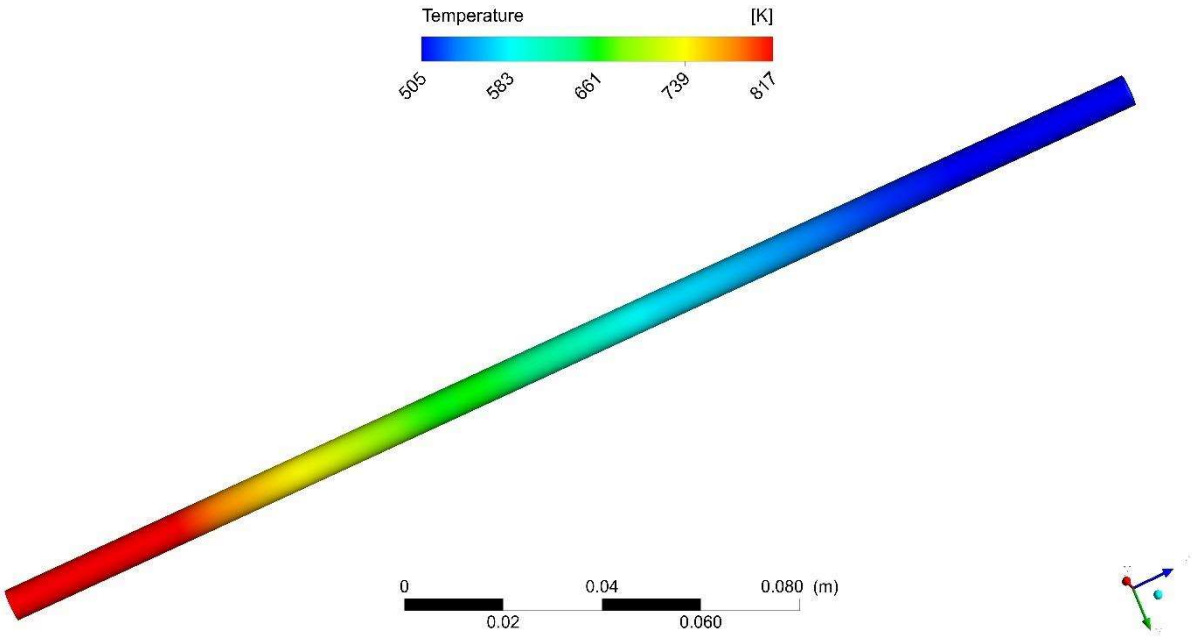


Figure 8. Temperature profile of the reactor obtained by CFD simulation. Reaction conditions: GHSV=11,520 $h^{-1}$, $T_{inlet}$=503 K, P=5 atm and $H_2/CO_2$ molar ratio=4.

The validation of the proposed reactor configuration was carried out under the simulated conditions. In this experiment, the operation of the reactor started by fixing the pressure at 5 atm, followed by setting the flow rate at the proposed GHSV of 11,520 $h^{-1}$ (F=930 $NmL \cdot min^{-1}$) and switching on the preheater to rise the inlet gas mixture temperature to the desired temperature of 503 K. At these conditions, the experimental temperature profile was quite similar as the simulated one, as shown in Figure 9. Accordingly, the technical feasibility of the reactor was experimentally validated at lab-scale, as no external heating or cooling was necessary. The experimental temperature was in the range of 830-495 K with a $CO_2$ conversion equal to 93%, very close to the simulated results. At the low temperature of the outlet, the chemical equilibrium is totally shifted to products. Thus, in principle 100% of conversion could be achieved at very high residence time (see equilibrium data in Figure S1). With regard to the total heat released to the ambient and $CH_4$ productivity rate obtained during the process, it was estimated for this proposed reactor design a total heat of 0.07 [-kW] and a $CH_4$ productivity rate of 95.68 $mol \cdot h^{-1} \cdot kg_{cat.}^{-1}$.

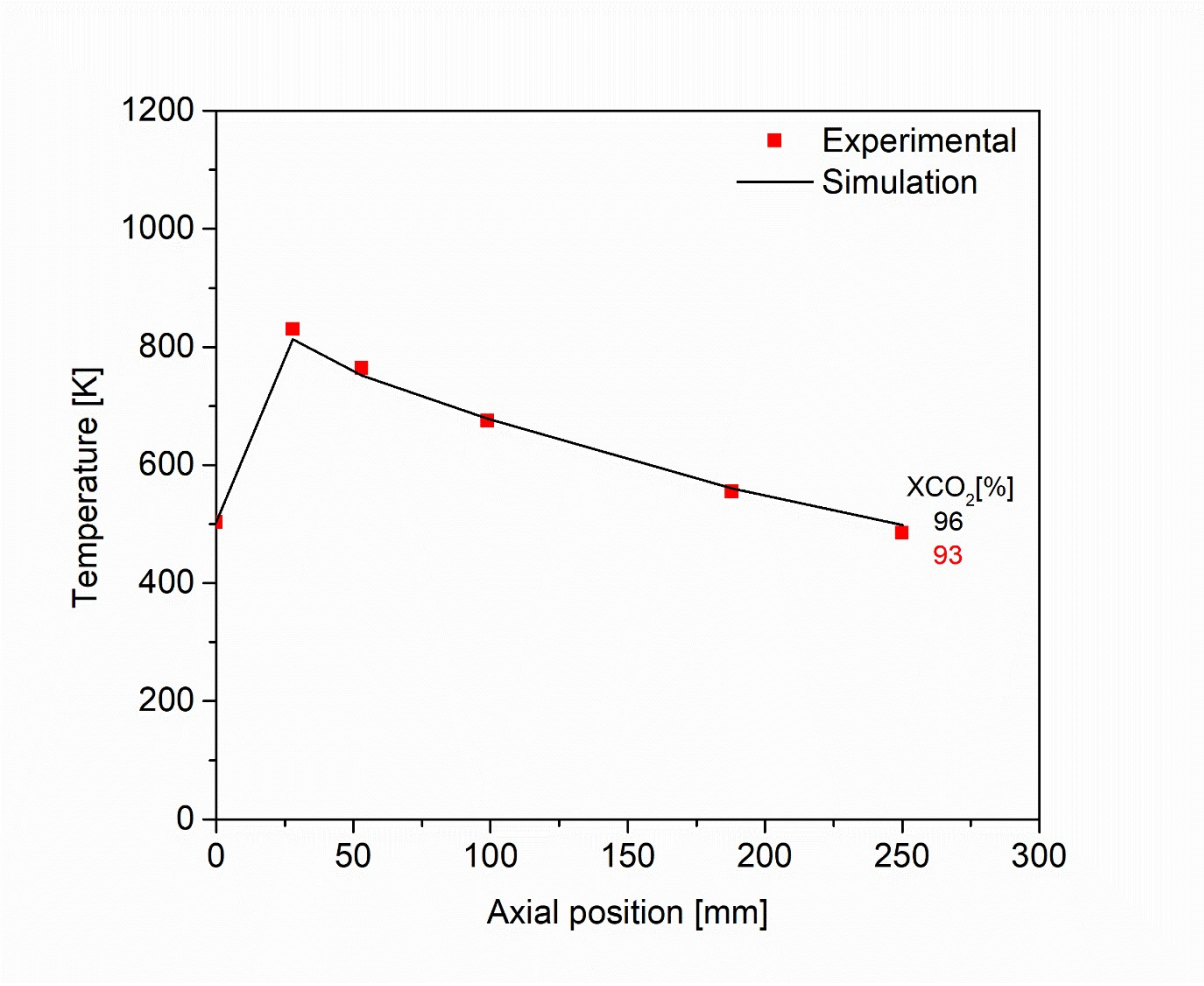


Figure 9. Experimental and simulation comparison of the proposed reactor conditions. GHSV=11,520 $h^{-1}$, $T_{inlet}$=503 K, P=5 atm and $H_2/CO_2$ molar ratio=4.

Considering that the proposed reactor design can be exposed to the unpredictable variations of the ambient air temperature ($T_{air}$), additional simulations were then performed to evaluate its effect on temperature profiles and $CO_2$ conversions. This set

of simulations was carried out in a $T_{air}$ range of 273 to 323 K. As is shown in Figure 10, the thermal operation performance of the proposed reactor design is slightly influenced by the $T_{air}$. An increase in the temperature along the reactor was detected as soon as the air temperature increases. Nevertheless, all temperatures ($T_{max}$≤827) and $CO_2$ conversions ($X_{CO2}$≥92%) were above the target criteria ($T_{max}$≤830 K and $X_{CO2}$≥90%). The most unfavourable result was observed when the $T_{air}$ was the too high, 323 K. At these environment conditions, $CO_2$ conversion was reduced by 4% and the temperature profile was in the range of 827 to 523 K. Consequently, it is inferred that $T_{air}$ can modify the behaviour of the proposed heat-management approach to a certain degree, which is obviously a drawback of the proposed configuration.

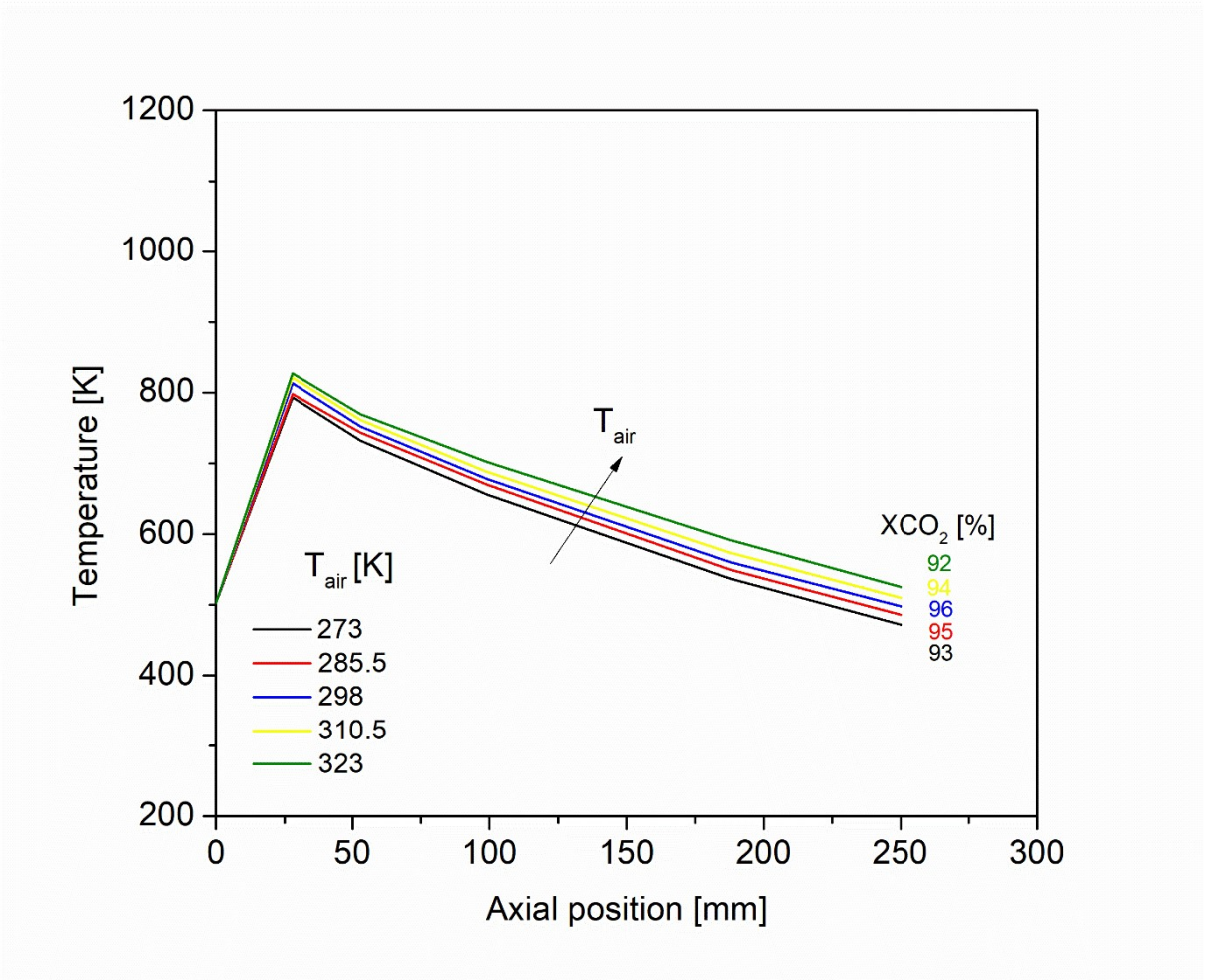


Figure 10. Influence of $T_{air}$ on the temperature profile and the conversion level at GHSV=11,520 h-1, $T_{inlet}$=503 K, P=5 atm and $H_2/CO_2$ molar ratio=4

### 4.5. Comparison with other heat-management approaches

The production of 1 $Nm^3 \cdot h^{-1}$ of SNG based on a pure $CO_2/H_2$ mixture was selected as the representative industrial small-scale $CO_2$ methanation case. According to the reactor dimensions (d=4.6 mm, L=250 mm), 23 channels will be required to achieve the targeted SNG production rate. It is important to point out that the reactor proposal even works at slightly higher GHSV values (11,520 $h^{-1}$) with respect to the commercial

technology (9,000 $h^{-1}$) at industrial scale [55]. On the contrary, at much lower GHSV values than the advanced micro-structured reactors (54,000 $h^{-1}$) [42] that are in a pre-commercialization state. This as simple as possible thermal approach requires of similar, or slightly lower, volume and catalyst amount than conventional multi-tubular reactors. Nevertheless, in a large-scale power-to-gas application the amount of tubes would be 30-fold larger, considering 25 mm diameter as standard tube diameter for conventional bundle reactors. In this sense, the amount of necessary auxiliaries would be lower, while the amount of tubes would be much larger due to the compromise between reduced dimensions of the tube diameter and operational GHSV values.

On the other hand, the steady-state temperature profile obtained during its experimental validation was reached after approximately 56 min, as it is shown in Figure 11. It is anticipated that the start-up of the proposed reactor is slower than reactors that include an internal heat exchange system. As an example, the start-up of a micro-structured reactor is carried out in approximately 8-30 min, using both heating and cooling auxiliaries [42]. Another aspect to consider in this heat-management approach is the reaction safety. Reactor runaway can occur in exothermic reactions because of irregular composition of the reactants or some fluctuation of inlet temperature. In those cases, an increase of the reaction temperature can change conditions in a way that it causes a further increase in temperature, leading to a destructive result. This fact can be problematic as no cooling system is proposed to actively control the reactor temperature. Fortunately, this undesired situation can be easily avoided by stopping the $CO_2$ dosage into the reactor and/or by injecting an auxiliary gas as nitrogen. As soon as no $CO_2$ is introduced to the reactor, the reactor temperature immediately drops.

In the present work, the main pros and cons of a heat-management for $CO_2$ methanation based on free convection were disclosed. The main advantage of the present approach is the simple design and low auxiliary requirements of this reactor, especially in decentralized locations where the integration of the exothermic heat to another industrial unit is not technically feasible or, more probably, not economically profitable. In this sense, the proposed reactor can be an alternative to consider for producing synthetic natural gas at reasonable GHSV in decentralized small-scale Power-to-Gas installations, as in most biogenic $CO_2$ sources.

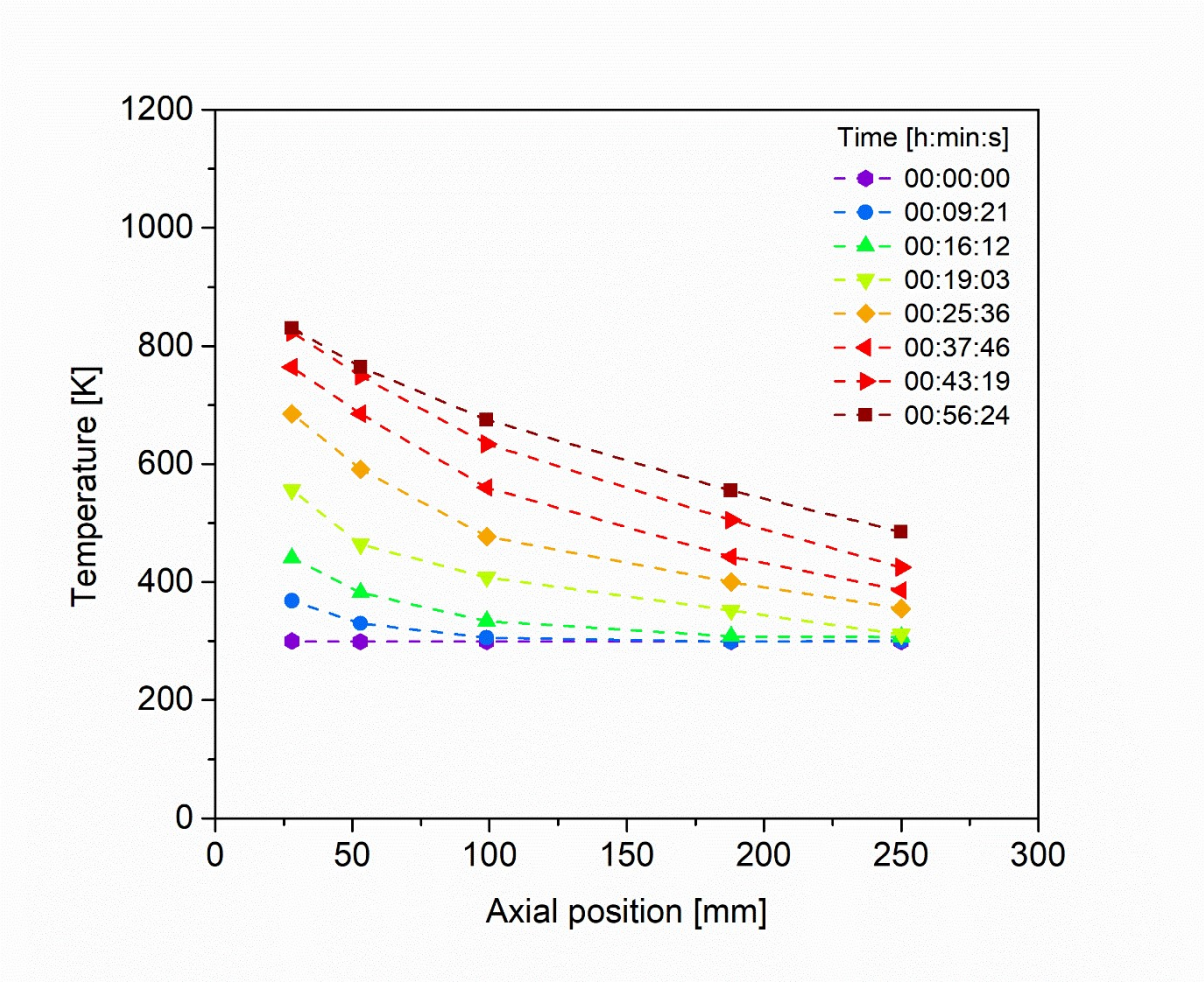


Figure 11. Experimental evolution of the temperature profile during the reaction start-up. Reaction conditions: GHSV=11,520 $h^{-1}$, $T_{inlet}$=503 K, P=5 atm and $H_2/CO_2$ molar ratio=4.

## 5. Conclusions

A reactor design using a simple heat-management based on free convention was proposal in this work. The application of this approach is intended for the small-size production of synthetic natural gas from $CO_2$ catalytic methanation. The technical feasibility of the proposed heat-management was studied through experimentation on a lab-scale single reactor channel (diameter of 4.6 mm and length of 250 mm) and conducing a sensitive analysis by means of a CFD model to disclose the most favourable reaction conditions.

The experimental results revealed that the reaction conditions should be carefully selected as no external heating or cooling units can be used to adjust the temperature profiles and thus to obtain high conversion levels. The experimental data was successfully described by means of the CFD model. Accordingly, CFD modelling appears as a powerful tool that can be used for the optimization of the reaction parameters, rather than excessive experimentation. The sensitive analysis conducted by CFD simulations showed that the operation of the reactor is feasible through a compromise between 3 operation parameters: gas hourly space velocity, inlet

494 temperature and pressure. In parallel, it was observed that the $T_{air}$ can have an
495 influence on the reactor yield.

496 The optimal conditions, which met $CO_2$ conversion higher than 90% and temperature
497 lower than 830 K criteria, were obtained by CFD simulation, and then, experimentally
498 validated. Those conditions were GHSV at 11,520 $h^{-1}$, inlet temperature of 503 K,
499 pressure of 5 atm, and air temperature of 298 K. Under those conditions, an interesting
500 level of $CO_2$ conversion (93%) was successfully achieved. The decreasing
501 temperature profile along the reactor was in the range of 830 to 495 K, without the
502 need of external heating or cooling units. Therefore, the proof-of-concept of the
503 operation for $CO_2$ methanation based on free convection is hereby validated in a single
504 channel reactor at lab-scale. According to the proposed reactor dimensions, 23
505 channels will be required to achieve the industrial small-scale production of 1 $Nm^3 \cdot h^{-1}$
506 of synthetic natural gas.

507

508 **Acknowledgements**

509 Authors thank Generalitat de Catalunya for financial support through the CERCA
510 Programme, M2E (2017SGR1246) and XaRMAE network. IREC also gratefully
511 acknowledge the funding of this work by the CoSin project (COMRDI15-1-0037),
512 funded by ACCIÓ and the European Regional Development Fund (ERDF) under the
513 framework of RIS3CAT Energy Community. Andreina Alarcón is grateful to Escuela
514 Superior Politécnica del Litoral (ESPOL) for the support during her postgraduate
515 studies ("Walter Valdano Raffo" Program, First edition).

516

517 **References**

518 [1] M. Lehner, R. Tichler, H. Steinmüller, M. Koppe, Power-to-Gas: Technology
519 and business models, Springer International Publishing, Cham, 2014.
520 doi:10.1007/978-3-319-03995-4.

521 [2] M. Götz, J. Lefebvre, F. Mörs, A. McDaniel Koch, F. Graf, S. Bajohr, R.
522 Reimert, T. Kolb, Renewable Power-to-Gas: A technological and economic
523 review, Renewable Energy. 85 (2016) 1371–1390.
524 doi:10.1016/j.renene.2015.07.066.

525 [3] J. Guilera, J. Ramon Morante, T. Andreu, Economic viability of SNG
526 production from power and CO 2, Energy Conversion and Management. 162
527 (2018) 218–224. doi:10.1016/j.enconman.2018.02.037.

528 [4] R.R. Boggula, D. Fischer, R. Casaretto, J. Born, Methanation potential:
529 Suitable catalyst and optimized process conditions for upgrading biogas to
530 reach gas grid requirements, Biomass and Bioenergy. 133 (2020) 105447.
531 doi:10.1016/j.biombioe.2019.105447.

532 [5] S. Bellocchi, M. De Falco, M. Gambini, M. Manno, T. Stilo, M. Vellini,
533 Opportunities for power-to-gas and power-to-liquid in CO2-reduced energy
534 scenarios: The Italian case, Energy. 175 (2019) 847–861.
535 doi:10.1016/j.energy.2019.03.116.

[6] J. Lindorfer, M. Lehner, D.C. Rosenfeld, B. Hans, Scenario analysis of implementing a power-to-gas and biomass gasification system in an integrated steel plant : A techno-economic and environmental study, Renewable Energy. 147 (2020) 1511–1524. doi:10.1016/j.renene.2019.09.053.

[7] X. Wang, Z. Bie, F. Liu, Y. Kou, L. Jiang, Bi-level planning for integrated electricity and natural gas systems with wind power and natural gas storage, International Journal of Electrical Power & Energy Systems. 118 (2020) 105738. doi:10.1016/j.ijepes.2019.105738.

[8] A. Basnet, J. Zhong, Electrical power and energy systems integrating gas energy storage system in a peer-to-peer community energy market for enhanced operation, Electrical Power and Energy Systems. 118 (2020) 105789. doi:10.1016/j.ijepes.2019.105789.

[9] R. Chauvy, L. Dubois, P. Lybaert, D. Thomas, G. De Weireld, Production of synthetic natural gas from industrial carbon dioxide, Applied Energy. 260 (2020) 114249. doi:10.1016/j.apenergy.2019.114249.

[10] A. Crivellari, V. Cozzani, Offshore renewable energy exploitation strategies in remote areas by power-to-gas and power-to-liquid conversion, International Journal of Hydrogen Energy. 45 (2020) 2936–2953. doi:10.1016/j.ijhydene.2019.11.215.

[11] A.K. Karmaker, M.M. Rahman, M.A. Hossain, M.R. Ahmed, Exploration and corrective measures of greenhouse gas emission from fossil fuel power stations for Bangladesh, Journal of Cleaner Production. 244 (2020) 118645. doi:10.1016/j.jclepro.2019.118645.

[12] A. Malara, P. Frontera, P. Antonucci, A. Macario, Smart recycling of carbon oxides: current status of methanation reaction, Current Opinion in Green and Sustainable Chemistry. (2020) 100376. doi:https://doi.org/10.1016/j.cogsc.2020.100376.

[13] P. Frontera, A. Macario, M. Ferraro, P. Antonucci, Supported Catalysts for CO2 Methanation: A Review, Catalysts. 7 (2017) 59. doi:10.3390/catal7020059.

[14] W. Wei, G. Jinlong, Methanation of carbon dioxide: an overview, Frontiers of Chemical Science and Engineering. 5 (2011) 2–10. doi:10.1007/s11705-010-0528-3.

[15] W. Ahmad, M.N. Younis, R. Shawabkeh, S. Ahmed, Synthesis of lanthanide series (La, Ce, Pr, Eu & Gd) promoted Ni/Γ-Al2O3 catalysts for methanation of CO2 at low temperature under atmospheric pressure, Catalysis Communications. 100 (2017) 121–126. doi:10.1016/j.catcom.2017.06.044.

[16] J. Liu, W. Shen, D. Cui, J. Yu, F. Su, G. Xu, Syngas methanation for substitute natural gas over Ni-Mg/Al2O3 catalyst in fixed and fluidized bed reactors, Catalysis Communications. 38 (2013) 35–39. doi:10.1016/j.catcom.2013.04.014.

[17] A. Zhao, W. Ying, H. Zhang, H. Ma, D. Fang, La and Mn promotion of Ni/Al2O3 catalysts for syngas methanation, Energy Sources, Part A: Recovery, Utilization and Environmental Effects. 36 (2014) 1049–1056.

580 doi:10.1080/15567036.2012.666621.

581 [18] J. Guilera, J. del Valle, A. Alarcón, J.A. Díaz, T. Andreu, Metal-oxide promoted
582 Ni/Al2O3 as CO2 methanation micro-size catalysts, Journal of CO2 Utilization.
583 30 (2019) 11–17. doi:https://doi.org/10.1016/j.jcou.2019.01.003.

584 [19] G. Garbarino, C. Wang, T. Cavattoni, E. Finocchio, P. Riani, M. Flytzani-
585 Stephanopoulos, G. Busca, A study of Ni/La-Al2O3 catalysts: A competitive
586 system for CO2 methanation, Applied Catalysis B: Environmental. 248 (2019)
587 286–297. doi:10.1016/j.apcatb.2018.12.063.

588 [20] L. Kiewidt, J. Thöming, Predicting optimal temperature profiles in single-stage
589 fixed-bed reactors for CO2-methanation, Chemical Engineering Science. 132
590 (2015) 59–71. doi:http://dx.doi.org/10.1016/j.ces.2015.03.068.

591 [21] M. Martinez Molina, C. Kern, A. Jess, Catalytic hydrogenation of carbon
592 dioxide to methane in wall-cooled fixed-bed reactors ‡, Chemical Engineering
593 & Technology. 39 (2016) 2404–2415. doi:10.1002/ceat.201500614.

594 [22] J. Bremer, H.G.R. Karsten, K. Sundmacher, CO2 Methanation : Optimal start-
595 up control of a fixed-bed reactor for power-to-gas applications, Amercian
596 Institute of Chemicals Engineerins. 63 (2017) 23–31. doi:10.1002/aic.

597 [23] J. Ducamp, A. Bengaouer, P. Baurens, Modelling and experimental validation
598 of a CO2 methanation annular cooled fixed-bed reactor exchanger, Canadian
599 Journal of Chemical Engineering. 95 (2017) 241–252. doi:10.1002/cjce.22706.

600 [24] C. Schüler, M. Wolf, O. Hinrichsen, Contactless temperature measurements
601 under static and dynamic reaction conditions in a single-pass fixed bed reactor
602 for CO2 methanation, Journal of CO2 Utilization. 25 (2018) 158–169.
603 doi:10.1016/j.jcou.2018.03.016.

604 [25] R. Currie, S. Mottaghi-tabar, Y. Zhuang, D.S.A. Simakov, Design of an air-
605 cooled Sabatier reactor for thermocatalytic hydrogenation of CO2 :
606 Experimental proof-of-concept and model- based feasibility analysis, Industrial
607 & Engineering Chemistry Research. 58 (2019) 12964–12980.
608 doi:10.1021/acs.iecr.9b01426.

609 [26] E. Giglio, F.A. Deorsola, M. Gruber, S.R. Harth, E.A. Morosanu, D. Trimis, S.
610 Bensaid, R. Pirone, Power-to-Gas through high temperature electrolysis and
611 carbon dioxide methanation: reactor design and process modeling, Industrial
612 and Engineering Chemistry Research. 57 (2018) 4007–4018.
613 doi:10.1021/acs.iecr.8b00477.

614 [27] N. Engelbrecht, S. Chiuta, R.C. Everson, H.W.J.P. Neomagus, D.G.
615 Bessarabov, Experimentation and CFD modelling of a microchannel reactor for
616 carbon dioxide methanation, Chemical Engineering Journal. 313 (2017) 847–
617 857. doi:10.1016/j.cej.2016.10.131.

618 [28] C. Jia, Y. Dai, Y. Yang, J.W. Chew, A fluidized-bed model for NiMgW-
619 catalyzed CO2 methanation, Particuology. 49 (2020) 55–64.
620 doi:10.1016/j.partic.2019.05.004.

621 [29] J. Lefebvre, N. Trudel, S. Bajohr, T. Kolb, A study on three-phase CO2
622 methanation reaction kinetics in a continuous stirred-tank slurry reactor, Fuel.

623 217 (2018) 151–159. doi:10.1016/j.fuel.2017.12.082.

624 [30] Y. Rodríguez-Guerra, L.A. Gerling, E.A. López-Guajardo, F.J. Lozano-García,
625 K.D.P. Nigam, A. Montesinos-Castellanos, Design of micro- and milli-channel
626 heat exchanger reactors for homogeneous exothermic reactions in the laminar
627 regime, Industrial & Engineering Chemistry Research. 55 (2016) 6435–6442.
628 doi:10.1021/acs.iecr.6b00323.

629 [31] R. Dittmeyer, T. Boeltken, P. Piermartini, M. Selinsek, M. Loewert, F.
630 Dallmann, H. Kreuder, M. Cholewa, A. Wunsch, M. Belimov, S. Farsi, P.
631 Pfeifer, Micro and micro membrane reactors for advanced applications in
632 chemical energy conversion, Current Opinion in Chemical Engineering. 17
633 (2017) 108–125. doi:10.1016/j.coche.2017.08.001.

634 [32] D. Türks, H. Mena, U. Armbruster, A. Martin, Methanation of CO2 on Ni/Al2O3
635 in a structured fixed-bed reactor—A scale-up study, Catalysts. 7 (2017) 152.
636 doi:10.3390/catal7050152.

637 [33] B. Kreitz, G.D. Wehinger, T. Turek, Dynamic simulation of the CO2
638 methanation in a micro-structured fixed-bed reactor, Chemical Engineering
639 Science. 195 (2019) 541–552. doi:10.1016/j.ces.2018.09.053.

640 [34] M. Neubert, A. Hauser, B. Pourhossein, M. Dillig, J. Karl, Experimental
641 evaluation of a heat pipe cooled structured reactor as part of a two-stage
642 catalytic methanation process in power-to-gas applications, Applied Energy.
643 229 (2018) 289–298. doi:https://doi.org/10.1016/j.apenergy.2018.08.002.

644 [35] S. Pérez, J.J. Aragón, I. Peciña, E.J. Garcia-Suarez, Enhanced CO2
645 methanation by new microstructured reactor concept and design, Topics in
646 Catalysis. (2019). doi:10.1007/s11244-019-01139-4.

647 [36] S. Neuberg, H. Pennemann, V. Shanmugam, R. Thiermann, R. Zapf, W. Gac,
648 M. Greluk, W. Zawadzki, G. Kolb, CO2 methanation in microstructured
649 reactors – catalyst development and process design, Chemical Engineering
650 and Technology. 42 (2019) 2076–2084. doi:10.1002/ceat.201900132.

651 [37] M. Belimov, D. Metsger, P. Pfeifer, On the temperature control in a micro
652 structured packed bed reactor for methanation of CO/CO2 mixtures, American
653 Institute of Chemical Engineers Journal. 61 (2014) 1–15. doi:10.1002/aic.

654 [38] D. Schollenberger, S. Bajohr, M. Gruber, R. Reimert, T. Kolb, Scale-up of
655 innovative honeycomb reactors for power-to-gas applications – The project
656 Store&Go, Chemie-Ingenieur-Technik. 90 (2018) 696–702.
657 doi:10.1002/cite.201700139.

658 [39] M. Gruber, C. Wieland, P. Habisreuther, D. Trimis, D. Schollenberger, S.
659 Bajohr, O. VonMorstein, S. Schirrmeister, Modeling and design of a catalytic
660 wall reactor for the methanation of carbon dioxide, Chemie Ingenieur Technik.
661 90 (2018) 615–624. doi:10.1002/cite.201700160.

662 [40] S. Rönsch, J. Schneider, S. Matthischke, M. Schlüter, M. Götz, J. Lefebvre, P.
663 Prabhakaran, S. Bajohr, Review on methanation – From fundamentals to
664 current projects, Fuel. 166 (2016) 276–296. doi:10.1016/j.fuel.2015.10.111.

665 [41] Z. Anxionnaz, M. Cabassud, C. Gourdon, P. Tochon, Heat exchanger /

reactors ( HEX reactors ): Concepts , technologies :, Chemical Engineering and Processing: Process Intensification. 42 (2008) 2029–2050.

[42] J. Guilera, T. Boeltken, F. Timm, I. Mallol, A. Alarcón, T. Andreu, Pushing the limits of SNG process intensification: high GHSV operation at pilot scale, Summited to ACS Sustainable Chemistry & Engineering. (2020).

[43] N. Engelbrecht, R.C. Everson, D. Bessarabov, Thermal management and methanation performance of a microchannel- based Sabatier reactor / heat exchanger utilising renewable hydrogen, 208 (2020).

[44] Z. Shao, S.M. Haile, J. Ahn, P.D. Ronney, Z. Zhan, S.A. Barnett, A thermally self-sustained micro solid-oxide fuel-cell stack with high power density, Nature. 435 (2005) 795–798. doi:10.1038/nature03673.

[45] B.F. Hagh, Optimization of autothermal reactor for maximum hydrogen production, International Journal of Hydrogen Energy. 28 (2003) 1369–1377. doi:10.1016/S0360-3199(02)00292-6.

[46] E. Moioli, N. Gallandat, A. Züttel, Model based determination of the optimal reactor concept for Sabatier reaction in small-scale applications over Ru/Al2O3, Chemical Engineering Journal. 371 (2019) 121954. doi:10.1016/j.cej.2019.121954.

[47] J. Bremer, K. Sundmacher, Operation range extension via hot-spot control for catalytic CO2 methanation reactors, Reaction Chemistry & Engineering. 4 (2019) 1019–1037. doi:10.1039/C9RE00147F.

[48] W. Zhang, H. Machida, H. Takano, K. Izumiya, K. Norinaga, Computational fluid dynamics simulation of CO2 methanation in a shell-and-tube reactor with multi-region conjugate heat transfer, Chemical Engineering Science. 211 (2020) 115276. doi:10.1016/J.CES.2019.115276.

[49] A. Alarcón, J. Guilera, J.A. Díaz, T. Andreu, Optimization of nickel and ceria catalyst content for synthetic natural gas production through CO2 methanation, Fuel Processing Technology. 193 (2019) 114–122. doi:10.1016/j.fuproc.2019.05.008.

[50] A. Alarcón, J. Guilera, R. Soto, T. Andreu, Higher tolerance to sulfur poisoning in CO2 methanation by the presence of CeO2, Applied Catalysis B: Environmental. 263 (2020) 118346. doi:10.1016/j.apcatb.2019.118346.

[51] A. Alarcón, J. Guilera, T. Andreu, CO2 conversion to synthetic natural gas: Reactor design over Ni–Ce/Al2O3 catalyst, Chemical Engineering Research and Design. (2018). doi:https://doi.org/10.1016/j.cherd.2018.10.017.

[52] J.J. Freeman, NIST Chemistry WebBook, SRD 69, National Institute of Standards and Technology. (2017). http://webbook.nist.gov/chemistry/ (accessed 11 July 1968).

[53] J. Guilera, T. Andreu, N. Basset, T. Boeltken, F. Timm, I. Mallol, J.R. Morante, Synthetic natural gas production from biogas in a waste water treatment plant, Renewable Energy. 146 (2020) 1301–1308. doi:10.1016/j.renene.2019.07.044.

[54] J. Gao, Y. Wang, Y. Ping, D. Hu, G. Xu, F. Gu, F. Su, A thermodynamic analysis of methanation reactions of carbon oxides for the production of